INTERNATIONAL JOURNAL OF HYDROGEN ENERGY 41 (2016) 14377–14386

Available online at www.sciencedirect.com

ScienceDirect

journal homepage: www.elsevier.com/locate/he

Reduction of CO_2 with KBH_4 in solvent-free conditions

Carolina V. Picasso [a,1], Damir A. Safin [a,1], Iurii Dovgaliuk [a], François Devred [a], Damien Debecker [a], Hai-Wen Li [b,c], Joris Proost [d], Yaroslav Filinchuk [a,*]

[a] Institute of Condensed Matter and Nanosciences, Université catholique de Louvain, Place L. Pasteur 1, B-1348 Louvain-la-Neuve, Belgium
[b] International Research Center for Hydrogen Energy, Kyushu University, Fukuoka 819-0395, Japan
[c] International Institute for Carbon-Neutral Energy Research (WPI-I2CNER), Kyushu University, Fukuoka 819-0395, Japan
[d] Institute of Mechanics, Materials and Civil Engineering, Université catholique de Louvain, Place Sainte-Barbe 2, B-1348 Louvain-la-Neuve, Belgium

ARTICLE INFO

Article history:
Received 31 December 2015
Accepted 8 April 2016
Available online 25 June 2016

Keywords:
CO_2 reduction
Potassium borohydride
Potassium triformylhydroborate
Crystal structure
Mechanochemistry
Solvent-free conditions

ABSTRACT

Metal hydrides have been commonly used as reducing agents in organic and inorganic chemistry. Until today, the capability of potassium borohydride (KBH_4) to reduce aldehydes and ketones to alcohols has been known for its advantage of high stability on air and in alkaline solutions. Conversion of CO_2 to formates and boron methoxide compounds by metal borohydrides has been recently studied. In this work we investigated the solid–gas non-catalytic reaction between KBH_4 and CO_2 under both mechanochemical and thermal-induced conditions with the simultaneous formation of potassium formylhydroborates, $K[H_xB(OCHO)_{4-x}]$ ($x = 1$–3), as main products. The first crystal structure of a product of solid–gas metal borohydride – CO_2 reaction, potassium triformylhydroborate, $K[HB(OCHO)_3]$, obtained mechanochemically, was elucidated. The evolution of the reaction between solid KBH_4 and CO_2 was monitored by a combination of thermogravimetric analysis coupled with mass spectrometry and infrared spectroscopy from room temperature to 500 °C, revealing the generation of hydrogen, methanol and carbon monoxide in a three-step mass increase reaction. Variable temperature *in situ* synchrotron X-ray powder diffraction under CO_2 pressure revealed the formation of a new crystalline intermediate phase with an unidentified composition but crystallizing in a monoclinic space group, and KBO_2 during the second and third steps, respectively. Gas chromatography of evolving species under CO_2 flow revealed for the first time the formation of methanol and methane in water-free conditions.

* Corresponding author.
E-mail address: yaroslav.filinchuk@uclouvain.be (Y. Filinchuk).
[1] These authors contributed equally to this work.
http://dx.doi.org/10.1016/j.ijhydene.2016.04.052

Introduction

Carbon dioxide (CO_2) is the most important long-lived greenhouse gas contributing to global climate change. In particular, this becomes even more crucial nowadays due to a dramatic increase in global fuel consumption leading to enormous emissions of CO_2. On the other hand, CO_2 is an attractive and easily available source as the C_1 building block for chemicals of value. Reduction of CO_2, which has been extensively investigated [1], is likely the most promising strategy to address both issues. The most popular methods for CO_2 reduction are metal- [2–5] or organo-catalyzed [6–14] hydroboration. These processes are, usually, efficient for producing formate [4] or its further reduction to give methoxy products [2,3,5–14]. The latter compounds are of particular interest due to being one step precursors for methanol through hydrolysis.

Recently, it was found that the phosphine-borane system in presence of hydroboranes is extremely efficient for producing methoxy products [15]. Furthermore, commercially available THF solution of borane, $H_3B{\cdot}THF$, which contains 0.5 mol % of sodium borohydride as a stabilizing reagent, reduces CO_2 to give trimetoxyboroxine [16]. The latter product is also formed in the reaction of pure $H_3B{\cdot}THF$ with CO_2, using a catalytic amount of sodium formate instead of $NaBH_4$ [16].

The first reports, describing the reactivity of metal borohydrides with CO_2, date to the 1950s. Heller et al. studied the reaction of $^{14}CO_2$ with lithium borohydride in ether and established the formation of lithium formate, diborane and MeOH as a minor product [17]. Later, Wartik and Pearson reported the absorption of CO_2 by $LiBH_4$ with formation of lithium formatotrimethoxyborate, $Li[B(OCH_3)_3(OCHO)]$, and $LiBO_2$, accompanied by a small quantity of B_2H_6 and dimethoxyborane, $BH(OCH_3)_2$, when the reaction was conducted at high temperature in the absence of solvent, while formation of $Li[BO(OCH_3)(OCHO)]$ was observed when the reaction was carried out in ether [18]. However, the sodium analog, $Na[BO(OCH_3)(OCHO)]$, was found to form in the absence of solvent upon reacting of $NaBH_4$ with CO_2, while the formation of $Na[HB(OCHO)_3]$ was established during the reaction in dimethyl ether [18,19]. A more recent paper also reports on the formation of $Na[HB(OCHO)_3]$, accompanied by $Na[H_2B(OCHO)_2]$, but during the reduction of CO_2 in acetonitrile [20]. The same conditions also favor the formation $NH_4[HB(OCHO)_3]$ when ammonium borohydride, NH_4BH_4, is treated with CO_2 [20]. In general, the interaction of $NaBH_4$ with CO_2 highly depends on the reaction conditions. For example, a THF solution of $NaBH_4$ in the presence of trimethylphosphine uptakes CO_2 with the formation of sodium formate and trimethylphosphine borane, $H_3B{-}P(CH_3)_3$ [21]. The former compound is also found upon reacting $NaBH_4$ and CO_2 in aqueous conditions [22]. There are several other works describing the reduction of CO_2 with $NaBH_4$ in aqueous media [23–25]. Furthermore, porous magnesium borohydride, γ-$Mg(BH_4)_2$, efficiently reacts with CO_2 with the formation of formate and alkoxide-like compounds with unprecedented fast kinetics at 30 °C and 1 bar [26,27].

Transition metal borohydrides were also found to be efficient for the direct reduction of CO_2 [28–39]. Among them copper borohydrides are the most studied [28–30,32–35]. An intriguing temperature-dependent formation of the $[HB(OCHO)_3]^-$ and $[H_2B(OCHO)_3]^{2-}$ species was established upon reacting $(phen)Cu(PPh_3)BH_4$ with CO_2 [33].

In the course of our comprehensive study of metal borohydrides for hydrogen storage, we have recently found that CO_2 significantly boosts up the hydrolysis reaction rates, transforming potassium borohydride into a new complex compound $K_9[B_4O_5(OH)_4]_3(CO_3)(BH_4){\cdot}7H_2O$ [40]. Furthermore, formic acid was found to be produced upon reduction of CO_2 using an aqueous solution of KBH_4 [41]. Herein, we report on the in-depth studies of direct reduction of CO_2 with KBH_4 under solvent-free mechanochemical and thermal-induced conditions. To the best of our knowledge, a catalysis- and solvent-free reaction between CO_2 and KBH_4 has not been reported so far. The latter circumstances are of great importance in the meaning of both green chemistry and proximity to the practical realities.

Experimental part

Mechanochemical solid–gas reaction of KBH_4 with CO_2

The mechanochemical synthesis by ball milling at 600 rpm was performed in a 80 mL stainless steel EASY GTM grinding bowl, equipped with a gas pressure and temperature measuring system for controlling the milling process, using a FRITSCH PULVERISETTE 7 premium line Planetary Ball Mill. KBH_4 (0.54 g) and solid CO_2 (1.7 g) under the nitrogen flow were loaded into the bowl with stainless steel balls (4 × 4 g, ø = 10 mm). The mixture was ball milled for 35 milling cycles, with a cycle duration of 5 min and a pause of 1 min, leading to the formation of a white mushy product.

Thermal-induced solid–gas reaction of KBH_4 with CO_2

The reaction was performed at 30, 50 and 90 °C and 25–30 bar of CO_2 using a tubular horizontal furnace, 4 cm^3 autoclave and a gas control system connected to a Keller pressure transducer with a 0.01% precision. KBH_4 (100–200 mg) was loaded under an argon atmosphere into a 40 × 8.2 mm borosilicate glass vial with glass wool on the top, placed inside the autoclave and connected to the gas control system.

NMR spectroscopy

NMR spectra in DMSO-d_6 were collected on a Bruker Avance DRX500 spectrometer operating at 500.133 MHz for ^1H, 125.770 MHz for ^{13}C and 160.462 MHz for ^{11}B nuclei. Chemical shifts are reported with reference to $SiMe_4$ for ^1H and ^{13}C and $BF_3{\cdot}OEt_2$ for ^{11}B.

Solid state NMR spectroscopy

^1H and ^{11}B NMR spectra were performed on a Bruker Ascend-600 spectrometer (14.1 T) operating at ^1H and ^{11}B Larmor frequencies of 600.130 MHz and 192.546 MHz, respectively, and were recorded with a 3.2 mm probe with 16 kHz magic angle spinning (MAS). Chemical shifts are reported with reference to $SiMe_4$ for ^1H and $BF_3{\cdot}OEt_2$ for ^{11}B.

Monitoring of the solid–gas reaction of KBH_4 with CO_2 using thermal gravimetric analysis coupled with mass spectrometry (TGA-MS)

TGA-MS analysis of the solid–gas reaction of KBH_4 with CO_2 was performed using a Mettler Toledo AG – TGA/SDTA851e instrument coupled with a ThermoStar GSD 301T spectrometer. Temperature was increased from room temperature to 500 °C with a heating rate of 2 °C/min, followed by an isothermal stabilization for 1 h at 500 °C. KBH_4 (20–25 mg) was loaded into a Al_2O_3 crucible and exposed to a dynamic CO_2 flow (25 mL/min) through the sample.

Monitoring of the solid–gas reaction of KBH_4 with CO_2 using thermal gravimetric analysis coupled with Fourier transform infrared spectroscopy (TGA-FTIR)

TGA-FTIR analysis of the gas phase of the solid–gas reaction of KBH_4 with CO_2 was performed using a Mettler Toledo AG – TGA/SDTA851e instrument coupled with a Nicolet Nexus 870 FTIR spectrometer. Temperature was increased from room temperature to 500 °C with a heating rate of 2 °C/min, followed by an isothermal stabilization for 1 h at 500 °C. KBH_4 (8.3 mg) was loaded into a Al_2O_3 crucible and exposed to a dynamic CO_2 flow (25 mL/min) through the sample.

Monitoring the solid–gas reaction of KBH_4 with CO_2 using volumetry

Volumetric analysis of the CO_2 uptake by KBH_4 was performed using a Hiden Isochema IMI-SHP analyzer at 30, 50 and 100 °C. KBH_4 (50–100 mg) was loaded into a reactor under an argon atmosphere and exposed to 1 bar of CO_2.

Monitoring of the solid–gas reaction of KBH_4 with CO_2 using gas chromatography (GC)

Crushed KBH_4 (0.14 g) was loaded into a fixed-bed micro-reactor and pretreated in helium at 120 °C for 2 h and then left under helium flow overnight at 50 °C prior to experiment. Then a CO_2 flow of 10 mL/min was admitted and the temperature was increased from 50 up to 500 °C with a heating rate of 2 °C/min. The gas phase of the solid–gas reaction of KBH_4 with CO_2 was analyzed by online gas chromatography, using a CP-3800 Varian apparatus equipped with a TCD and a FID detectors. The analysis parameters were set up to allow one analysis of the gas phase every 8.5 min.

Monitoring of the solid–gas reaction of KBH_4 with CO_2 using variable temperature in situ synchrotron X-ray powder diffraction (SR-XPD)

Synchrotron radiation powder diffraction data were collected at varied temperatures at the Materials Science Beamline at PSI (Villigen, Switzerland), using Mythen II detector and $\lambda = 0.775045$ Å. Temperature was increased linearly in time from room temperature to 492 °C with a 5 °C/min heating rate. Ground KBH_4 was filled under high purity argon atmosphere into a 0.5 mm sapphire capillary and sealed. The capillary was connected to a gas dosing system and exposed to CO_2 at 30 bar.

Variable temperature in situ synchrotron X-ray powder diffraction and crystal structure determination

The crystal structure of $K[HB(OCHO)_3]$ was solved from *in situ* SR-XPD data collected from the ball milled sample at SNBL/ESRF (Grenoble, France) with a PILATUS 2M pixel detector and $\lambda = 0.68857$ Å. The ground sample was filled under high purity argon atmosphere into a 0.5 mm sapphire capillary sealed with vacuum grease. Temperature was increased linearly in time, using Oxford Cryostream 700+, from room temperature to 500 °C with a 10 °C/min heating rate. The 2D images were azimuthally integrated using the Fit2D software and LaB_6 as a standard [42]. For the structure solution 19 diffraction peaks were indexed using DICVOL [43] in a primitive monoclinic cell. Le Bail fit and analysis of systematic absences suggested the monoclinic space group $P2_1/c$. The structure was solved by global optimization in direct space using FOX [44]. The position of the potassium atom and the position and orientation of OCHO groups were optimized. Once the geometry of the $[HB(OCHO)_3]^-$ anion was recognized in the partially solved structure, the anion was parameterized with z-matrix. For that, bond distances and angles were approximated by those optimized in the program HyperChem [45]. Flexible automatic restraints on bond distances and angles in the anion were applied, antibump restraints were also included. The final refinement was performed by the Rietveld method (Fig. S1 in Supplementary data) using the program Fullprof [46]. The coordinates of all atoms were refined using 13 bond distance and 18 angle restraints. Isotropic atomic displacement factor was refined for the potassium atom and one group atomic displacement for all other atoms, arriving to reasonable values. The background was described by linear interpolation between selected points. The contribution from the cubic KBH_4 phase was successfully modeled by the Le Bail fit. The final discrepancy factors are $R_B = 10.6\%$, $R_F = 9.7\%$, $R_p = 2.1\%$ and $R_{wp} = 2.7\%$.

Results and discussion

The reaction of solid KBH_4 with solid CO_2 under mechanochemical conditions, performed in a stainless steel grinding bowl with stainless steel balls, yields a white mushy product, which is readily soluble at least in DMSO-d_6 with the negligible release of gas bubbles. It should be noted that using tungsten carbide bowl and balls (2×8 g, ø = 10 mm) leads to the same product, which identity was established by means of NMR spectroscopy.

The ^{11}B NMR spectrum of the obtained product in DMSO-d_6 exhibits a dominating quintet at −35.6 ppm, with a characteristic coupling constant $^1J_{B,H} = 81.2$ Hz, corresponding to the BH_4^- anion (Fig. 1). The low field part of the ^{11}B NMR spectrum contains one quartet ($^1J_{B,H} = 96.2$ Hz), one triplet ($^1J_{B,H} = 116.1$ Hz) and one doublet ($^1J_{B,H} = 130.5$ Hz) at −9.5, 1.1 and 3.5 ppm, respectively, which were assigned to the

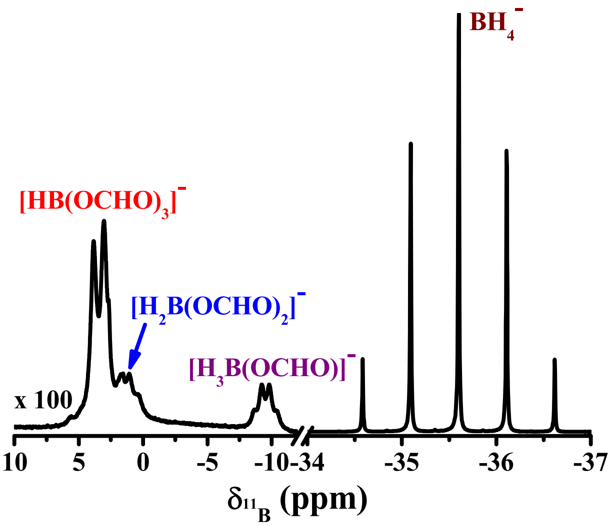

Fig. 1 – The ^{11}B NMR spectrum of the product obtained after ball milling.

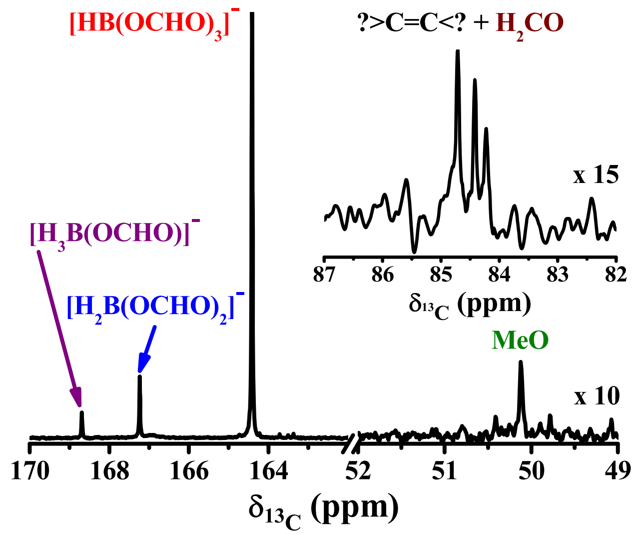

Fig. 2 – The $^{13}C\{^1H\}$ NMR spectrum of the product obtained after ball milling.

$[H_3B(OCHO)]^-$, $[H_2B(OCHO)_2]^-$ and $[HB(OCHO)_3]^-$ anions, respectively (Fig. 1) [20]. The latter two signals are significantly overlapped. The observed coupling constants of all multiplets were proved to be of the $^1J_{B,H}$ nature by recording $^{11}B\{^1H\}$ spectra, where all signals turned to singlets. Besides all, the ^{11}B NMR spectrum contains a broad singlet centered at about 18.5 ppm (not shown in Fig. 1 to keep it eye-catching), which can be assigned to the boron nuclei in the O_3 environment, e.g. trimethyl borate $B(OMe)_3$, which formation is also suggested from the TGA-MS data described below, and/or KBO_2 [47]. Furthermore, the ^{11}B NMR spectrum also exhibits a negligible singlet signal with a very low intensity at about 5.7 ppm (Fig. 1), which can be tentatively assigned to the boron nuclei in the O_4 environment, e.g. the tetramethoxyborate anion $[B(OMe)_4]^-$. The ^{13}C NMR spectrum of the same product contains sharp peaks at 164.2, 167.0 and 168.5 ppm, assigned to the $[HB(OCHO)_3]^-$, $[H_2B(OCHO)_2]^-$ and $[H_3B(OCHO)]^-$ anions, respectively (Fig. 2) [20]. The spectrum also exhibits four singlets at 50.1, 84.2, 84.4 and 84.7 ppm. The former peak corresponds to the methoxide carbon atom, while the latter three peaks can, most likely, be assigned to formaldehyde and ethylene-based species. The ^1H NMR spectrum of the ball milled product shows a 1:1:1:1 quartet centered at −0.35 ppm corresponding to the BH_4^- protons (Fig. 3). Since boron compounds naturally contain two NMR active isotopes, the splitting pattern for the BH_4^- anion exhibits the intense quartet arising from ^1H and ^{11}B coupling with $^1J_{11B,H} = 81.1$ Hz, as well as the less pronounced septet due to ^1H and ^{10}B coupling with $^1J_{10B,H} = 27.2$ Hz (Fig. 3). $[H_3B(OCHO)]^-$, $[H_2B(OCHO)_2]^-$ and $[HB(OCHO)_3]^-$ anions are shown in the ^1H NMR spectrum as corresponding singlets of the OCHO protons at 8.04, 8.13 and 8.22 ppm, respectively. Furthermore, the former two anions are also found as characteristic four-line splitting patterns centered at 3.72 and 2.16 ppm, respectively, corresponding to the borohydride protons, while the BH proton of the latter anion is situated somewhere between and is significantly overlapped with other signals (Fig. 3). The spectrum also contains sharp peaks at 3.0–3.2 and 4.5–5.0 ppm, which can be due to the presence of formaldehyde, and ethylene- and (−CH−O−)-based species. It should be noted, that, based on the relative integral intensities of the peaks of the OCHO protons, the prevailing formation of the $[H_3B(OCHO)]^-$ anion (100%) was found compared to $[H_2B(OCHO)_2]^-$ (12%) and $[HB(OCHO)_3]^-$ (6%). Interestingly, the ^1H NMR spectrum of the sample, obtained after 1 h of ball milling, in DMSO-d_6 contains characteristic peaks for MeOH: a doublet and a quartet at 3.13 and 4.06 ppm, respectively, with a characteristic coupling constant $^3J_{H,H} = 5.3$ Hz. The formation of MeOH is also reflected in the ^{13}C NMR spectrum in the same solvent as a singlet at 49.2 ppm. Furthermore, the ^1H NMR spectrum of the same sample also exhibits a singlet at 4.59 ppm, corresponding to molecular hydrogen. Finally, the ^{11}B, ^{13}C and ^1H NMR spectra of the sample, obtained after 1 h ball milling, contain sets of characteristic peaks, attributed to the $[H_3B(OCHO)]^-$, $[H_2B(OCHO)_2]^-$ and $[HB(OCHO)_3]^-$ anions.

We have further collected variable temperature SR-XPD data for the ball milled product with the aim to determine crystal structures of the formed products. As a result, the crystal structure of the $[HB(OCHO)_3]^-$ anion containing compound, namely $K[HB(OCHO)_3]$, was successfully established. It was found that $K[HB(OCHO)_3]$ crystallized in the monoclinic space group $P2_1/c$. The boron atom is in a pseudotetrahedral environment formed by three oxygen atoms of three OCHO fragments, and one hydride hydrogen (Fig. 4). All B–O bond distances are in the range of 1.47–1.49 Å, and the B–H bond length is about 1.22 Å. The bridging C–O(B) distances are about 1.33 Å, while the terminal C=O bonds are significantly shorter and of ~1.24 Å. The H–B–O bond angles range from 109.6 to 114.2°, while the O–B–O bond angles are somewhat smaller and span from 102.7 to 108.2°. The C–O–B angles deviates significantly and are of 116.5–125.5°. All O–C–O and H–C–O bond angles are close to 120°. Each $[HB(OCHO)_3]^-$ anion is μ^6-coordinated towards six potassium atoms through the oxygen atoms of the OCHO pendants and BH hydrogen atom with the

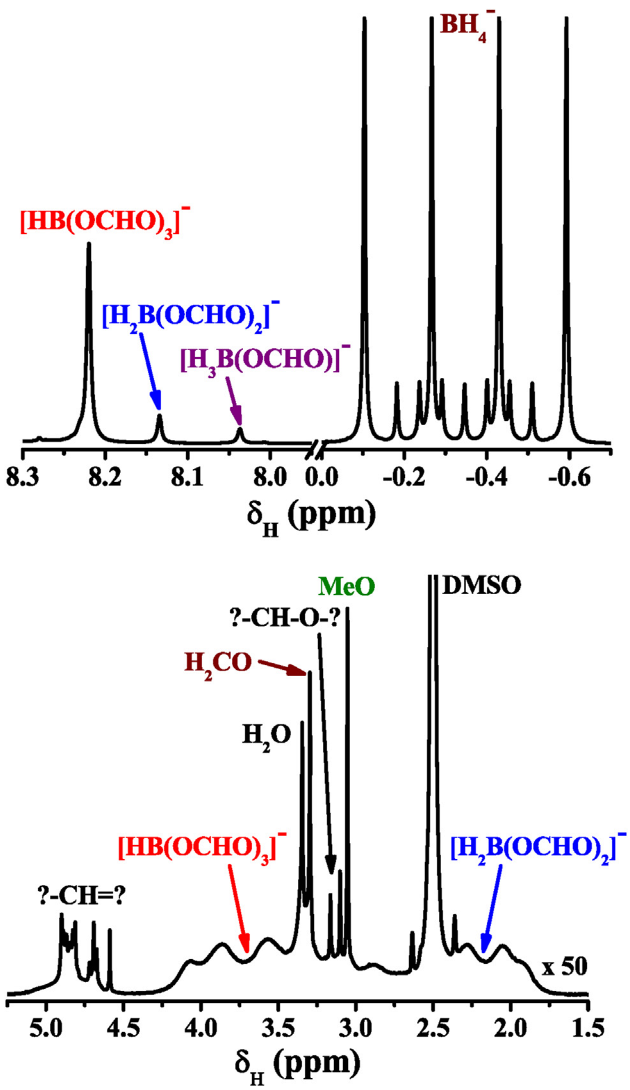

Fig. 3 – The ^{1}H NMR spectrum of the product obtained after ball milling. The cut out part of the spectrum is shown in the bottom graph.

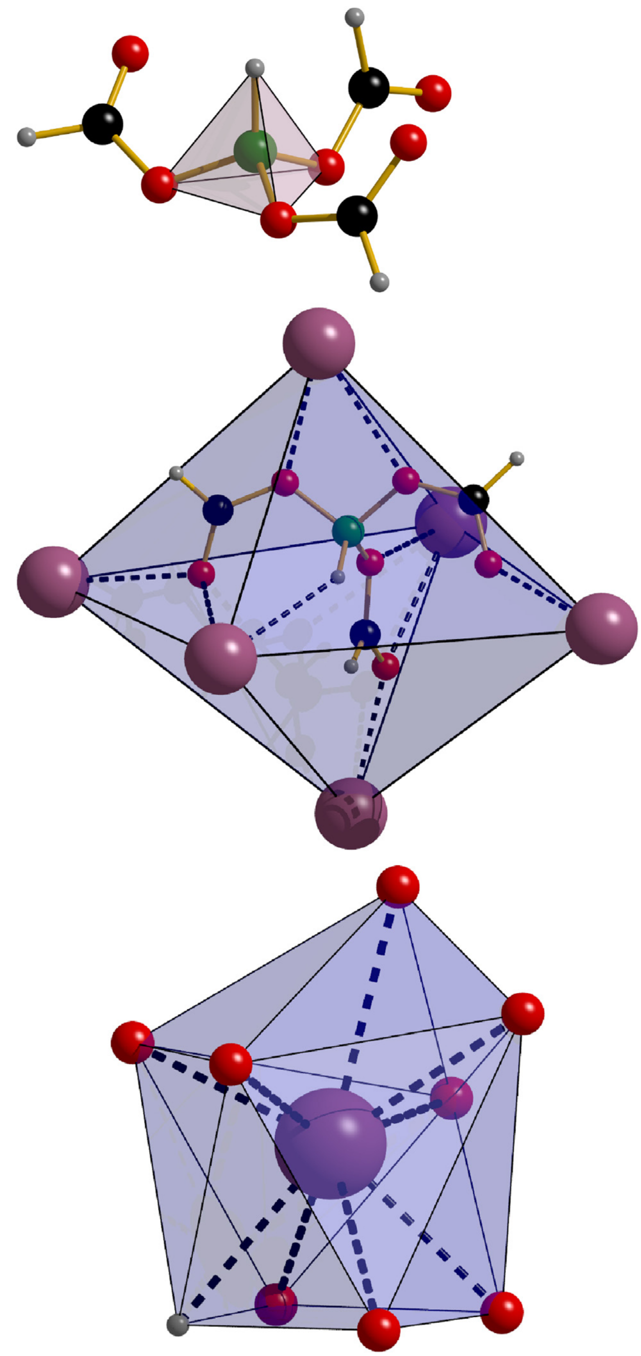

Fig. 4 – Molecular structure of the $[HB(OCHO)_3]^-$ anion (top), its coordination environment formed by the K^+ cations (middle), and coordination environment around the K^+ cation (bottom) as seen in the crystal structure of $K[HB(OCHO)_3]$. Color code: B = green, C = black, H = gray, K = purple, O = red. (For interpretation of the references to color in this figure legend, the reader is referred to the web version of this article.)

formation of a distorted coordination octahedron (Fig. 4). The K–O distances are 2.71–3.14 Å, while the K–H bond is about 2.83 Å. Interestingly, the $[HB(OCHO)_3]^-$ anion coordinates K^+ through both the terminal (C=O) and bridging (C–O–B) oxygen atoms. Furthermore, one of the pendant OCHO fragments coordinates the potassium atom through formation of the bidentate H–B–O–C–O chelate backbone (Fig. 4). The coordination environment around the K^+ cation is best described as a distorted monocapped square antiprism (Fig. 4). The overall structure of $\{K[HB(OCHO)_3]\}_n$ is a three-dimensional polymer constructed from two-dimensional alternating layers of the $[HB(OCHO)_3]^-$ anions and potassium cations (Fig. 5).

The crystal structure of $K[HB(OCHO)_3]$, to the best of our knowledge [48], is only the second structurally characterized example of the formylhydroborate anions after $\{Na(DME)[HB(OCHO)_3]\}_n$ [20]. Moreover, the structure of $K[HB(OCHO)_3]$ is the first example of non-solvated formylhydroborate salts exhibiting a rich and unique coordination mode of the anion.

The solid–gas reaction of KBH_4 with CO_2 was investigated in parallel by *in situ* TGA-MS (Fig. 6) and TGA-FTIR (Fig. 7) upon

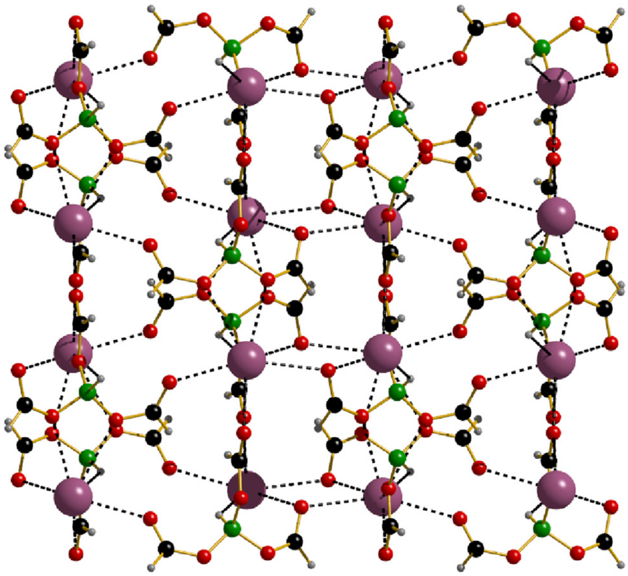

Fig. 5 – Crystal packing of {K[HB(OCHO)$_3$]}$_n$ along the c axis. Color code: B = green, C = black, H = gray, K = purple, O = red. (For interpretation of the references to color in this figure legend, the reader is referred to the web version of this article.)

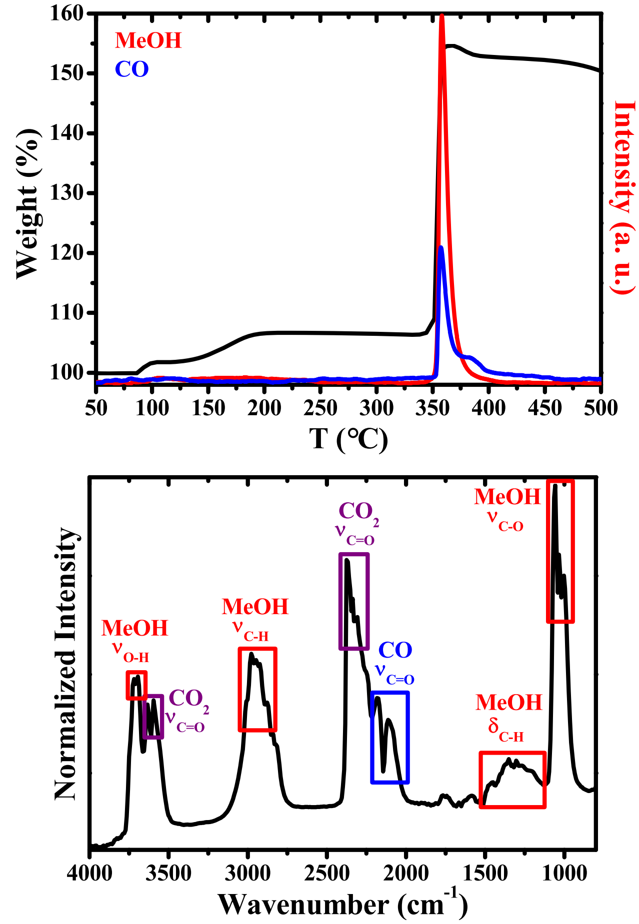

Fig. 7 – TGA-FTIR of the solid–gas reaction of KBH_4 with CO_2 (top) and the FTIR spectrum of the gas products formed at 360 °C (bottom), the temperature is plotted for the reference curve.

heating from room temperature to 500 °C in order to examine the gas phase products. It was found that KBH_4 reacts with CO_2 exhibiting three mass increase steps at about 90, 160 and 350 °C with the final residue corresponding to the formation of potassium metaborate (KBO_2). While the first two mass increase steps are gradual, the third step is abrupt and accompanied by a remarkable increase of the temperature followed by its stabilization (Figs. 6 and 7). The latter effect is explained by the exothermic reaction during the third mass increase step. A similar dramatic and abrupt mass increase during the last reaction step has also been observed in the reactions of $TiCl_3$-doped alanates (Li/NaAlH$_4$) with CO_2, suggesting that transition metal dopants enhance the reaction kinetics [49].

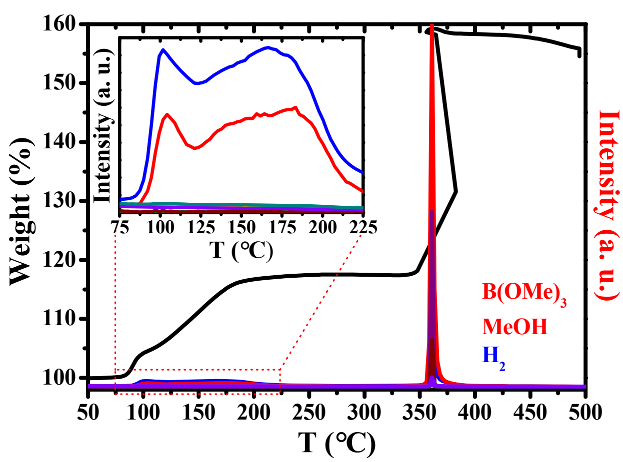

Fig. 6 – TGA-MS of the solid–gas reaction of KBH_4 with CO_2.

Thus, the third abrupt mass increase step upon reacting of KBH_4 with CO_2 under *in situ* TGA-MS (Fig. 6) and TGA-FTIR (Fig. 7) experimental conditions, reveals an enhanced reaction kinetics.

According to the TGA-MS data, all mass increase steps, and in particular the third step, are accompanied by the simultaneous evolution of H_2 and, most likely, B(OMe)$_3$ (Fig. 6). The release of the latter product is supported by the presence of characteristic *m/z* peaks 15, 29, 30, 31, 72, 73 and 104 in TGA-MS. However, the formation of MeOH can also contribute into the *m/z* peaks 15, 29, 30, 31.

Monitoring of the solid–gas reaction of KBH_4 with CO_2 using TGA-FTIR allowed to observe the simultaneous formation of MeOH and CO during the third mass increase step at about 350 °C (Fig. 7). It should be noted that CO is produced from 350 to 400 °C with two maxima at about 355 and 375 °C, while MeOH appears from about 350 to 375 °C. Furthermore, the formation of borates is also possible when heating up to higher temperatures. However, the characteristic IR bands of borates are in the same region as for MeOH and, thus, cannot be firmly identified. This can be further supported by a relatively low concentration of borates.

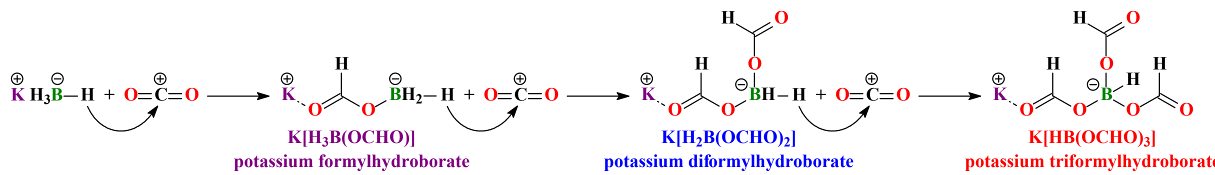

Scheme 1 – Formation of formylhydroborates upon reacting KBH_4 with CO_2.

We have then performed volumetric analysis of the CO_2 uptake by KBH_4 at 30, 50 and 100 °C (Fig. S2 in Supplementary data). It was found that both at 30 and 50 °C the amount of absorbed CO_2 is very similar and of about 200 mmol CO_2 per 1 mol of KBH_4. However, the activation time of the reaction is significantly shorter at 50 °C (~40 min) compared to that at 30 °C (~7 h). The reaction at 100 °C has no activation time but a pronounced reduction of the volume increase is observed (Fig. S2 in Supplementary data). This is due to the evolution of volatile products during the reaction over ~90 °C as it has been observed during monitoring of the reaction using TGA-MS (Fig. 6).

The solid–gas reaction of KBH_4 with CO_2 was also monitored by means of GC. It was found that MeOH is formed upon heating from about 100 °C to 350 °C with a release maximum at about 225 °C, while the formation of CH_4 was observed in the temperature range of 275–500 °C with a release maximum at about 320 °C (Fig. S3 in Supplementary data). The productivity of MeOH is about 1000 times higher than of CH_4 at their corresponding release maxima.

The formation of formylhydroborate compounds upon reacting KBH_4 with CO_2 is most likely due to the hydride transfer, occurring from a hydroborate compound with or without the implication of the countercation (Scheme 1) [50]. The unprecedented formation of such volatile compounds as formaldehyde, MeOH and CH_4 can be initiated by boryl radicals, formed through the homolytic dissociation of the B–H bonds [51].

We have also calculated the standard free energy changes as a function of temperature for the hypothetic reactions $KBH_4 + CO_{2(g)} = CH_{4(g)} + KBO_2$ and $KBH_4 + 2CO_{2(g)} = CH_3OH_{(liq)} + KBO_2 + CO_{(g)}$ using the data source [52]. According to the obtained thermodynamic results it was established that the formation of both MeOH and CH_4 is energetically possible during the whole temperature range from 25 to 500 °C, with the formation of MeOH being remarkably less favored in comparison to CH_4 (Fig. 8). However, the preferred formation of MeOH followed by the formation of CH_4, as evidenced from the GC data (Fig. S3 in Supplementary data), can be explained by different reaction rates.

The evolution of crystalline phases upon heating KBH_4 under 30 bar of CO_2 was studies *in situ* by SR-XRPD. An intermediate phase appears at about 148 °C and disappears at about 231 °C (Fig. 9). It corresponds to the first plateau in the TGA data taken under CO_2 atmosphere (Fig. 7). KBH_4 remains the main crystalline phase up to approximately 350 °C, when the formation of KBO_2 starts. KBH_4 is present in the sample up to the highest temperature of the experiment, 500 °C. The reaction kinetics is apparently controlled by the diffusion of CO_2 into the solid state. A small amount of potassium formate is observed in a HCOOK:KBH_4 ≈ 1:50 weight ratio at temperatures close to the stability region of the intermediate phase.

For a more detailed structural study, the intermediate phase was obtained using the autoclave synthesis by keeping KBH_4 at 116 °C under 32 bar of CO_2 for 140 min. XRPD revealed a major contribution of the intermediate phase, along with HCOOK and KBO_2 in a 1:2 weight ratio. The peaks of the intermediate phase were indexed in the monoclinic unit cell with $a = 16.2315(3)$, $b = 7.39226(15)$, $c = 14.8587(3)$ Å, $\beta = 105.6330(14)°$, $V = 1716.91(6)$ Å^3 at room temperature. The systematic absences and the profile fit (Fig. S4 in Supplementary data) suggested the monoclinic space groups $C2/c$ or Cc. Our numerous attempts to solve the crystal structure of the intermediate phase failed. However, this sample was studied by means of ^1H and $^{11}B\{^1H\}$ MAS solid state NMR spectroscopy. The ^1H solid-state NMR spectrum exhibits three main broad singlets centered at 2.9, 5.6 and 8.3 ppm corresponding to the MeO methyl protons, HCOOK and $[H_xB(OCHO)_{4-x}]^-$ (x = 1–3) formate groups, respectively (Fig. 10). Remaining two broad singlets at around 0 ppm were attributed to the BH_4^- protons. The $^{11}B\{^1H\}$ MAS NMR spectrum of the same sample contains two broad singlets centered at 1.1 and 18.3 ppm (Fig. 10). The high-field signal corresponds to boron nuclei of the $[HB(OCHO)_3]^-$, $[H_2B(OCHO)_2]^-$ and $[H_3B(OCHO)]^-$ anions, while the low-field signal is due to the boron nuclei in the O_3 environment, e.g. trimethyl borate $B(OMe)_3$ as it was suggested for the $^{11}B\{^1H\}$ NMR spectrum of

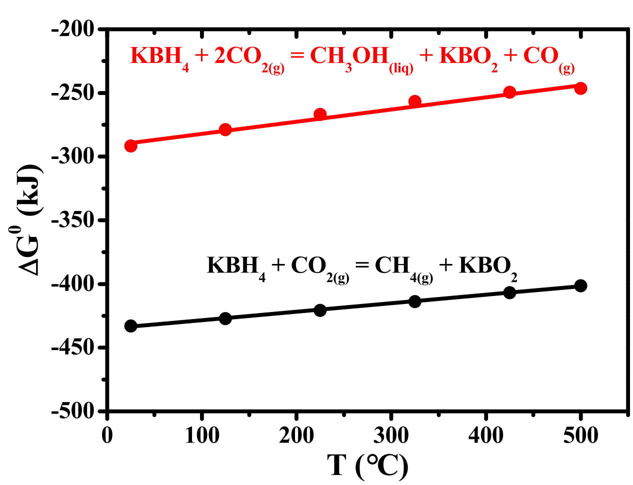

Fig. 8 – Calculated standard free energy changes as a function of temperature for 2 possible routes of CO_2 uptake by KBH_4 using the data source [52].

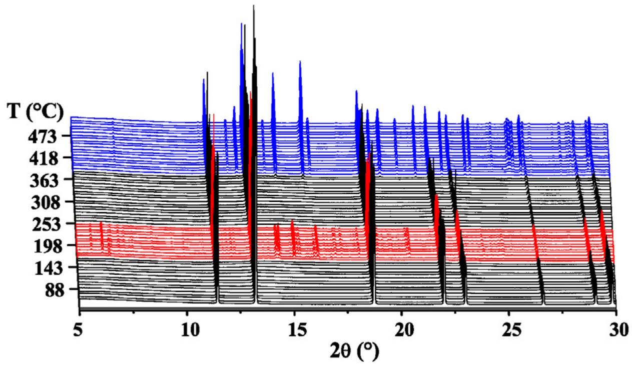

Fig. 9 – Variable temperature *in situ* synchrotron X-ray powder diffraction ($\lambda = 0.775045$ Å) of KBH_4 under the CO_2 atmosphere (30 bar).

the sample, obtained through ball milling, in DMSO-d_6. Another singlet peak was observed at about −38 ppm, which corresponds to the BH_4^- group. Furthermore, the $^{11}B\{^1H\}$ MAS NMR spectrum of the sample also exhibits peaks centered at about 9.0, 13.0 and 27.2 ppm, which assignment remains challenging. Thus, solid state NMR spectroscopy data echo the NMR data recorded in solution.

Another sample was prepared by keeping KBH_4 at 60 °C under 26 bar of CO_2 for 90 min. XRPD revealed that a major part of KBH_4 transformed into the intermediate phase. SR-XRD measurement on this sample under inert atmosphere showed an anisotropic unit cell expansion for the intermediate phase, followed by its disappearance at 175 °C, and the formation of the crystalline KBO_2 at 350 °C. The profile fit at 108 °C (Fig. S5 in Supplementary data) yielded the unit cell parameters $a = 16.2647(2)$, $b = 7.45594(17)$, $c = 14.9230(3)$ Å, $\beta = 105.3970(16)°$, $V = 1744.74(6)$ Å^3. We have attempted to

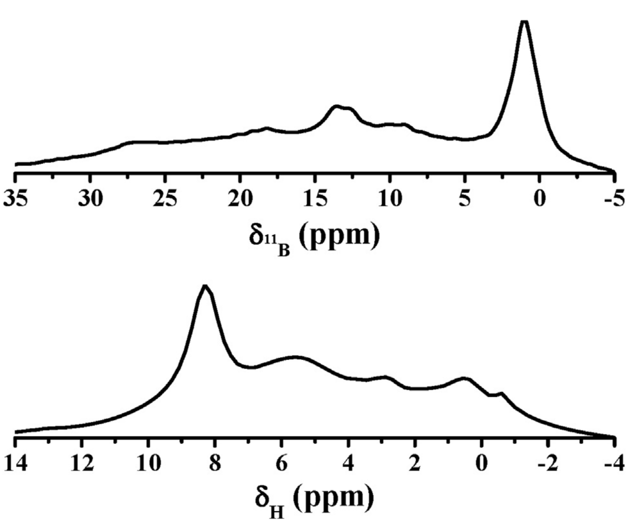

Fig. 10 – ^1H (bottom) and $^{11}B\{^1H\}$ (top) solid-state NMR spectra of the sample obtained in autoclave synthesis by keeping KBH_4 at 116 °C under 32 bar of CO_2 for 140 min; the corresponding diffraction data are shown in Fig. S4 in Supplementary data.

solve the structure using simultaneously data collected at different temperatures, thus reducing the effective peaks' overlap; however without success.

Variable temperature *in situ* SR-XRPD on the sample containing K[HB(OCHO)$_3$] show that its peaks disappear at about 87 °C and the intermediate phase forms at about 112 °C, vanishing at approximately 162 °C. These transformations occurring in the absence of CO_2, suggest a similarity between the two crystalline phases and/or an easy transformation of the chemically bound CO_2 within the molecular species.

Conclusions

In summary, we have reported a comprehensive study of the solid–gas non-catalytic reaction between a complex hydride (KBH_4) and CO_2 under both mechanochemical and thermal-induced conditions for the first time. The formation of potassium formylhydroborates, K[H$_x$B(OCHO)$_{4-x}$] ($x = 1$–3), as main products, was established. The crystal structure of the main product, which was obtained mechanochemically, namely potassium triformylhydroborate K[HB(OCHO)$_3$], was elucidated using synchrotron X-ray powder diffraction. The evolution of the reaction between solid KBH_4 and CO_2 was monitored by a combination of thermogravimetric analysis coupled with mass spectrometry and infrared spectroscopy from room temperature to 500 °C, revealing the generation of hydrogen, methanol and carbon monoxide in a three-step mass increase reaction. Variable temperature *in situ* synchrotron X-ray powder diffraction under the CO_2 pressure reveals the formation of a new crystalline intermediate phase with an unidentified composition but crystallizing in a centered monoclinic space group with the unit cell volume of 1716.91(6) Å^3, and KBO_2 during the second and third steps, respectively. Gas chromatography of evolving species under the CO_2 flow reveals the formation of methanol and methane in water-free conditions for the first time. The obtained formylhydroborates are of interest for the noncatalytic fabrication of hydrogen upon hydrolysis, which proceeds much more efficiently for the formylhydroborates in comparison with the parent borohydride (not reported in this work). A possible continuation of this project can be seen in establishing optimal conditions for a selective and sustainable generation of organic fuels or useful organics by recycling CO_2 with complex hydrides.

Acknowledgment

The authors thank FNRS (CC 1.5169.12, PDR T.0169.13, EQP U.N038.13) for financial support. We acknowledge WBI for the incoming postdoctoral fellowship for D. A. Safin and the Fonds Spéciaux de Recherche (UCL) for funding of the PhD fellowship of I. Dovgaliuk, and for the bridge funding for C. V. Picasso. We thank ESRF (Grenoble, France) for the beam time allocation at the SNBL, as well as PSI for the beam time at the MS beamline at SLS. The research leading to these results has received funding from the European Community's Seventh Framework Programme (FP7/2007–2013) under grant agreement n. 312284

(CALIPSO). This work was partially supported by the COST Action MP1103 "Nanostructured materials for solid-state hydrogen storage". We thank JSPS KAKENHI Grant Number 15K14168 and JSPS Invitation Fellowship for the short term research in Japan and the International Institute for Carbon Neutral Energy Research (WPI-I2CNER), sponsored by the Japanese Ministry of Education, Culture, Sports, Science and Technology. Mrs. Sabine Bebelman is thanked for her help with TGA-FTIR measurements.

Appendix A. Supplementary data

Supplementary data related to this article can be found at http://dx.doi.org/10.1016/j.ijhydene.2016.04.052.

REFERENCES

[1] Wang W, Wang S, Ma X, Gong J. Recent advances in catalytic hydrogenation of carbon dioxide. Chem Soc Rev 2011;40:3703–27.

[2] Chakraborty S, Zhang J, Krause JA, Guan H. An efficient nickel catalyst for the reduction of carbon dioxide with a borane. J Am Chem Soc 2010;132:8872–3.

[3] Sgro MJ, Stephan DW. Frustrated lewis pair inspired carbon dioxide reduction by a ruthenium tris(aminophosphine) complex. Angew Chem Int Ed 2012;51:11343–5.

[4] Shintani R, Nozaki K. Copper-catalyzed hydroboration of carbon dioxide. Organometallics 2013;32:2459–62.

[5] Abdalla JAB, Riddlestone IM, Tirfoin R, Aldridge S. Cooperative bond activation and catalytic reduction of carbon dioxide at a group 13 metal center. Angew Chem Int Ed 2015;54:5098–102.

[6] Menard G, Stephan DW. Room temperature reduction of CO_2 to methanol by Al-based frustrated lewis pairs and ammonia borane. J Am Chem Soc 2010;132:1796–7.

[7] Courtemanche M-A, Larouche J, Legare M-A, Bi W, Maron L, Fontaine F-G. A tris(triphenylphosphine)aluminum ambiphilic precatalyst for the reduction of carbon dioxide with catecholborane. Organometallics 2013;32:6804–11.

[8] Menard G, Stephan DW. CO_2 reduction *via* aluminum complexes of ammonia boranes. Dalton Trans 2013;42:5447–53.

[9] Wang T, Stephan DW. Phosphine catalyzed reduction of CO_2 with boranes. Chem Commun 2014;50:7007–10.

[10] Legare M-A, Courtemanche M-A, Fontaine F-G. Lewis base activation of borane-dimethylsulfide into strongly reducing ion pairs for the transformation of carbon dioxide to methoxyboranes. Chem Commun 2014;50:11362–5.

[11] Fontaine F-G, Courtemanche M-A, Legare M-A. Transition-metal-free catalytic reduction of carbon dioxide. Chem – Eur J 2014;20:2990–6.

[12] Wang T, Stephan DW. Carbene-9-BBN ring expansions as a route to intramolecular frustrated lewis pairs for CO_2 reduction. Chem – Eur J 2014;20:3036–9.

[13] Das Neves Gomes C, Blondiaux E, Thuery P, Cantat T. Metal-free reduction of CO_2 with hydroboranes: two efficient pathways at play for the reduction of CO_2 to methanol. Chem – Eur J 2014;20:7098–106.

[14] Courtemanche M-A, Legare M-A, Maron L, Fontaine F-G. Reducing CO_2 to methanol using frustrated lewis pairs: on the mechanism of phosphine-borane-mediated hydroboration of CO_2. J Am Chem Soc 2014;136:10708–17.

[15] Courtemanche M-A, Legare M-A, Maron L, Fontaine F-G. A highly active phosphine-borane organocatalyst for the reduction of CO_2 to methanol using hydroboranes. J Am Chem Soc 2013;135:9326–9.

[16] Fujiwara K, Yasuda S, Mizuta T. Reduction of CO_2 to trimethoxyboroxine with BH_3 in THF. Organometallics 2014;33:6692–5.

[17] Burr Jr JG, Brown WG, Heller HE. The reduction of carbon dioxide to formic acid. J Am Chem Soc 1950;72:2560–2.

[18] Wartik T, Pearson RK. Reactions of carbon dioxide with sodium and lithium borohydrides. J Inorg Nucl Chem 1958;7:404–11.

[19] Wartik T, Pearson RK. A new type of substituted borohydride. J Am Chem Soc 1955;77:1075.

[20] Knopf I, Cummins CC. Organometallics 2015;34:1601–3.

[21] Schmidbaur H, Weib E, Muller G. Synthesis of functional methylphosphane-borane derivatives I. convenient syntheses of tirmethylphosphane-borane and trimethylphosphane-monohaloboranes. Synth React Inorg Met Chem 1985;15:401–13.

[22] Eisenberg Jr F, Bolden AH. Formate contamination in borohydride reduction. Carbohydr Res 1967;5:349–50.

[23] Pulidindi IN, Kimchi BB, Gedanken AJ. Selective chemical reduction of carbon dioxide to formate using microwave irradiation. CO_2 Util 2014;7:19–22.

[24] Zhao Y, Zhang Z, Qian X, Han Y. Properties of carbon dioxide absorption and reduction by sodium borohydride under atmospheric pressure. Fuel 2015;142:1–8.

[25] Grice KA, Groenenboom MC, Manuel JDA, Sovereign MA, Keith JA. Examining the selectivity of borohydride for carbon dioxide and bicarbonate reduction in protic conditions. Fuel 2015;150:139–45.

[26] Filinchuk Y, Ban V, Jorgensen SW, Richter B, Jensen TR, Hudson MR, et al. Interaction of fuel gases with nanoporous γ-$Mg(BH_4)_2$. In: International symposium on metal-hydrogen systems (MH2012), Kyoto, Japan; Oct. 21–26, 2012. p. 330.

[27] Vitillo JG, Groppo E, Bardají EG, Baricco M, Bordiga S. Fast carbon dioxide recycling by reaction with γ-$Mg(BH_4)_2$. Phys Chem Chem Phys 2014;16:22482–6.

[28] Beguin B, Denise B, Sneeden RPA. Hydrocondensation of CO_2: II. Reaction of carbon dioxide and carbon monoxide with $[HCuPPh_3]_6$. J Organomet Chem 1981;208:C18–20.

[29] Bianchini C, Ghilardi CA, Meli A, Midollini S, Orlandini A. Facile reduction of carbon dioxide, carbonyl sulfide, and carbon disulfide by copper(I) borohydride. X-ray crystal structure of the complex $[(triphos)Cu(O_2CH)]$. J Organomet Chem 1983;248:C13–6.

[30] Bianchini C, Ghilardi CA, Meli A, Midollini S, Orlandini A. Reactivity of the tetrahydroborate copper(I) complexes $[(PR_3)_2Cu(\eta^2\text{-}BH_4)]$ (R = Ph, Cy) toward CO_2, COS, and SCNPh. J Organomet Chem 1983;255:C27–30.

[31] Willis W, Nicholas KM. The reactions of bis(tricyclohexylphosphine)-rhodium(I)carbonyl tetrahydridoborate with carbon dioxide and formic acid. Inorg Chim Acta 1984;90:L51–3.

[32] Bianchini C, Ghilardi CA, Meli A, Midollini S, Orlandini A. Reactivity of copper(I) tetrahydroborates toward carbon dioxide and carbonyl sulfide. Structure of $(triphos)Cu(\eta^1\text{-}O_2CH)$. Inorg Chem 1985;24:924–31.

[33] La Monica G, Ardizzoia G, Cariati F, Cenini S, Pizzotti M. Isolation of ionic products in the reaction of carbon dioxide with (tetrahydroborato)copper(I) complexes: synthesis and reactions of $[(biL)(Ph_3P)_2Cu][HB(O_2CH)_3]$ and $[(biL)(Ph_3P)_2Cu][H_2B(O_2CH)_2]$ (biL = 1,10-phenanthroline, 3,4,7,8-tetramethyl-1,10-phenanthroline). Inorg Chem 1985;24:3920–3.

[34] La Monica G, Angaroni MA, Franco C, Cenini S. Reactions of CO_2 with tetrahydroborato copper(I) complexes in moist

solvents: synthesis and reactions of [(phen)$_2$Cu][(HO)$_3$B(O$_2$CH)] and (phen)(Ph$_3$P)Cu(O$_2$COH) (phen = 1,10-phenanthroline). Inorg Chim Acta 1988;143:239–45.
[35] Pandey KK, Garg KH, Tiwari SK. Insertion reactions of carbonyl sulphide, carbon disulphide and carbon dioxide in the metal-hydrogen bond. Polyhedron 1992;11:947–50.
[36] Yi CS, Liu N. Ruthenium-mediated hydrogenation of carbon dioxide by $NaBH_4$ via the formation of the formate complex $C_5Me_5Ru(PCy_3)(\eta^2$-OCHO). Organometallics 1995;14:2616–7.
[37] Dionne M, Hao S, Gambarotta S. Preparation and characterization of a new series of Cr(II) hydroborates. Can J Chem 1995;73:1126–34.
[38] Journaux Y, Lozan V, Klingele J, Kersting B. Stabilisation of a paramagnetic BH_4^--bridged dinickel(II) complex by a macrodinucleating hexaaza-dithiophenolate ligand. Chem Commun 2006;219:83–4.
[39] Chakraborty S, Zhang J, Patel YJ, Krause JA, Guan H. Pincer-ligated nickel hydridoborate complexes: the dormant species in catalytic reduction of carbon dioxide with boranes. Inorg Chem 2013;52:37–47.
[40] Dovgaliuk I, Hagemann H, Leyssens T, Devillers M, Filinchuk Y. CO_2-promoted hydrolysis of KBH_4 for efficient hydrogen co-generation. Int J Hydrogen Energy 2014;39:19603–8.
[41] Fletcher C, Jiang Y, Amal R. Production of formic acid from CO_2 reduction by means of potassium borohydride at ambient conditions. Chem Eng Sci 2015;137:301–7.
[42] Hammersley AP, Svensson SO, Hanfland M, Fitch AN, Häusermann D. Two-dimensional detector software: from real detector to idealised image or two-theta scan. High Press Res 1996;14:235–48.
[43] Boultif A, Louer D. Powder pattern indexing with the dichotomy method. J Appl Crystallogr 2004;37:724–31.
[44] Favre-Nicolin V, Černý R. FOX, 'free objects for crystallography': a modular approach to *ab initio* structure determination from powder diffraction. J Appl Cryst 2002;35:734–43.
[45] HyperChem(TM) Professional 6.0, Hypercube, Inc., 1115 NW 4th Street, Gainesville, Florida 32601, USA.
[46] Rodríguez-Carvajal J. Recent advances in magnetic structure determination by neutron powder diffraction. Phys B 1993;192:55–69.
[47] Kroeker S, Stebbins JF. Three-coordinated boron-11 chemical shifts in borates. Inorg Chem 2001;40:6239–46.
[48] CSD version 5.36 updates. April 2015.
[49] Hugelshofer CL, Borgschulte A, Callini E, Matam SK, Gehrig J, Hog DT, et al. Gas-solid reaction of carbon dioxide with alanates. J Phys Chem C 2014;118:15940–5.
[50] Bontemps S. Boron-mediated activation of carbon dioxide. Coord Chem Rev 2016;308:117–30.
[51] Hioe J, Karton A, Martin JML, Zipse H. Borane-lewis base complexes as homolytic hydrogen atom donors. Chem Eur J 2010;16:6861–5.
[52] HSC Chemistry 6.12 (Outotec, Oberursel, Germany).